Title
Identifying Important Microphysical Properties and Processes for Marine Fog Forecasts

Journal
Monthly Weather Review, 151(9)

ISSN
0027-0644

Authors
Pope, Nathan Hexum
Igel, Adele L

Publication Date
2023-09-01

DOI
10.1175/mwr-d-22-0294.1

Identifying Important Microphysical Properties and Processes for Marine Fog Forecasts

Nathan Hexum Pope[a] Adele L. Igel[a,b]

[a] *Atmospheric Science Graduate Group, University of California, Davis,*[b] *Department of Land, Air and Water Resources, University of California, Davis*

Corresponding author: Nathan Hexum Pope, nhpope@ucdavis.edu

ABSTRACT: In this study, a marine fog event that occurred from 0000 to 1800 UTC on 7 September 2018 near Canada's Grand Banks is used to investigate the sensitivity of simulated fog properties to six model parameters found primarily in the microphysics scheme. To do so, we ran a large suite of regional simulations that spanned the life cycle of the fog event using the Regional Atmospheric Modeling System (RAMS). We randomly selected parameter combinations for the simulation suite and used Gaussian Process Regression to emulate the response of a variety of simulated fog properties to the parameters. We find that the microphysics shape parameter, which controls the relative width of the droplet size distribution, and the aerosol number concentration have the greatest impact on fog in terms of spatial extent, duration, and surface visibility. In general, parameters that reduce mean fall speed of droplets and/or suppress drizzle formation lead to reduced visibility in fog but also delayed onset, shorter lifetimes, and reduced spatial extent. The importance of the distribution width suggests a need for better characterization of this property for fog droplet distributions and better treatment of this property in microphysics schemes.

1. Introduction

Marine fog is a major meteorological hazard. Total annual economic losses due to fog can be comparable to hurricanes (Gultepe et al. 2007). An out-sized proportion of maritime accidents occur in the presence of fog (Gultepe et al. 2009), including the sinking of the RMS Titanic (Koračin 2017). The loss of the Titanic prompted GI Taylor to study fog off of Canada's Atlantic coast, culminating in *The Formation of Fog and Mist* (Taylor 1917). Taylor hypothesized that marine fog forms in regions with high sea surface temperature gradients due to the advection of warm, moist air over cold water. This "cold sea" or warm-air modification advection mechanism of marine fog formation is viewed as the most common type of marine fog (Lewis et al. 2004; Gultepe et al. 2007; Koračin et al. 2014). Willett (1928) discusses additional fog formation mechanisms, including cold and warm sea advection fog, and frontal fog. Frontal fog can form in a variety of ways. It is sometimes "precipitation fog", which forms when precipitation cools and/or moistens the boundary layer to saturation (Goldman 1951; Tardif 2007; Tardif and Rasmussen 2008, 2010). Alternatively, Anderson (1931) found that turbulent mixing within stratus clouds lowered cloud base and led to fog formation. Oliver et al. (1978) and Pilié et al. (1979) further studied this "stratus lowering fog", and Pilié et al. (1979) concluded that it is one of the most common fog formation mechanisms in California.

Globally, marine fog occurs most often near western ocean boundary currents. Specifically, fog is most common where these warm currents interact with protected regions of cold water (Lewis et al. 2004; Gultepe et al. 2007; Koračin 2017). Understanding marine fog formation near Canada's Grand Banks is particularly important due to the prevalence of fog as well as its importance as a shipping lane. The 2018 C-Fog campaign provided an extensive observational dataset with the aim of improving understanding of coastal and marine fog in the Grand Banks (Dorman et al. 2021a). Contrary to Taylor's hypothesis, the C-Fog data shows that most fog in the region results from large-scale cyclonic systems, with surface-level advection playing a minor role (Dorman et al. 2021b). Boutle et al. (2010) found that mid-latitude cyclonic systems provide a ready supply of moisture to the boundary layer through convergence, which can form fog as described in Fernando et al. (2021). Stratus lowering fog was found to be common in the Grand Banks. Many studies on stratus lowering fog have focused on the California coast (Pilié et al. 1979; Leipper 1994; Koračin et al. 2001, 2005a) and have found that radiative cloud-top cooling is the primary driver of fog formation. The findings of Wagh et al. (2021) for Atlantic Canada agree, noting that stratus lowering fog cases during the C-Fog campaign were related to cloud top cooling, stability, and entrainment at the top of the boundary layer.

Marine fog is a modeling challenge due to the number of possible formation mechanisms, such as warm advection over cold water, cold advection over warm water, and downward growth of low clouds. Different physical processes are important for different types of fog, and fog in general is sensitive to minor variations in temperature, moisture, and wind (Lewis et al. 2004; Koračin et al. 2005b; Gultepe et al. 2007; Koračin et al. 2014; Koračin 2017). Many marine fog studies have focused on cold sea advection fog, providing understanding on its sensitivity to sea surface temperature, wind profiles, and radiative and turbulent parameterizations (Fu et al. 2010; Heo and Ha 2010; Kim and Yum 2012, 2013; Huang et al. 2015). Microphysical impacts on fog have been investigated through observational (Gultepe et al. 1996; Duynkerke 1999; Zhao et al. 2013; Haeffelin et al. 2010; Niu et al. 2012) and modeling (Gultepe and Milbrandt 2007; Tardif and Rasmussen 2010) studies. Gultepe and Milbrandt (2007) found that accurate parameterization of microphysical properties helped improve the accuracy of fog simulations. Studies of radiation fog over land find that higher aerosol concentration and larger diameter favor fog formation (Koračin 2017; Boutle et al. 2018), but the dependence varies based on the type of fog being considered (Niu et al. 2012). Haeffelin et al. (2010) found that radiation fog and cloud base lowering fog near Paris probably had different, uncertain sensitivities to microphysics. Different possible formation mechanisms and their corresponding microphysical dependencies mean that the sensitivity of marine fog to microphysics is still an active area of research. Boutle et al. (2022) found that different models vary significantly in their prediction of fog.

This paper aims to address the uncertain relationship between microphysics and ~~marine fog~~ important properties of marine fog including spatial and temporal extent through sensitivity testing. The goal is to better constrain the response and response mechanisms of cyclonic marine fog in the Grand Banks variations in a set of microphysical parameters. We have identified a fog case that is characteristic of the Grand Banks, as well as several microphysical parameters and one surface flux parameter that may be impactful. We then sample the parameter space to create a suite of simulations that we use to explore the relationships between our input parameters and several output variables meant to characterize fog formation~~and evolution~~, evolution, and dissipation. In this way, we can identify which microphysical parameters are most important for fog in the Grand Banks region. This can be extended to shed light on the physics of fog formation, or on improving model parameterizations for more accurate forecasting.

2. Experimental Design

There were four major challenges when designing our experiment: choice of fog case, sampling of the parameter space, choosing output variables to quantify fog, and fitting those output variables to our input parameters. ~~Fog case choice needs to strike a balance between selecting a fog case that is representative of fog~~ Our choice of fog case needs to faithfully represent fog in the region ~~that can also be easily recreated in our model without using excessive computational resources. We need to~~ while also being simple to simulate to conserve computation time when running a large number of simulations. We also sample the multi-dimensional space defined by ~~our~~ the input parameters to capture ~~all~~ behavior while limiting the number of simulations~~that we need to run~~. Our output variables need to describe fog formation and evolution using ~~0-D data points~~summary quantities such as average visibility and extent. To construct relationships between input and output variables, we need to capture non-linearity and interactions between our parameters with strong prediction strength without over-fitting.

a. Fog Case

Fog in the Grand Banks is often related to a cyclonic system. Dorman et al. (2021b) found that every significant fog event recored at Ferryland on the island of Newfoundland, close to the Grand Banks, was related to a cyclonic system. Additionally, individual fog events at Ferryland lasted up to 31 hours continuously (Dorman et al. 2021b). Measuring fog events at fixed points will also tend to underestimate fog duration due to advection of the fog system. For this study, we adopt the view that a fog event begins when fog forms anywhere within the region of study (rather than being advected into the domain) and ends when fog completely dissipates completely.

Since this study examines marine fog specifically, and not coastal fog, in situ observations, such as those in the ICOADS database (ICO 2018) were sparse. Instead, we analyzed ERA5 (Hersbach et al. 2020) hourly reanalysis data for the Grand Banks region east of Newfoundland. The primary variable used to identify fog from ERA5 data was cloud base height. We assumed that any cloud base height below 30 m is probable fog. We also checked the 2 m relative humidity and 1000 mb cloud liquid water concentration to confirm the presence of fog. Most potential fog cases identified from ERA5 reanalysis following the above method agreed with the findings of Dorman et al. (2021b) in that they were related to cyclonic systems in the region.

Many of the fog events over the Grand Banks persist for several days from their initial formation until complete dissipation, even if they are only present for several hours at a fixed point. These are unsuitable because they occur over a very large area for a very long time, and thus are impractical for simulating repeatedly. Most short-lived events are very patchy, making them difficult to replicate in a model.

The fog case we chose occurred between 0000 and 1800 UTC on 7 September, 2018. Fog formed behind a fast-moving, low pressure system that passed East of Newfoundland, forming fog primarily over the cold waters of the Grand Banks. Fog occurred in several small-to-medium sized patches that overlapped temporally. There was one primary fog patch that grew the largest and persisted for around six hours. All fog in the event formed and completely dissipated ~~or moved out of the domain~~ within the an 18-hour life-cycle.

The case was simulated using the Regional Atmospheric Modeling System (RAMS; Cotton et al. 2003). The simulation domain is shown in ~~??e~~figure 1. In order to ensure that the simulations would run reasonably quickly, we used a moderate 5km spacing in the horizontal. In the vertical, we used 51 levels with 7 levels in the bottom 150 m where the spacing between the lowest levels was 10 m. A 5 second time step was used. Parameterization schemes included the LEAF3 surface scheme (Walko et al. 2000), the Harrington radiation scheme (Harrington 1997), a Smagorinsky-based subgrid mixing scheme (Smagorinsky 1963), and RAMS double-moment microphysics (Saleeby and van den Heever 2013). Sea surface temperatures were provided by the Reynolds daily sea surface temperature dataset (Reynolds et al. 2007) and were interpolated in time. Initial conditions and boundary nudging conditions were provdied by the ERA5 reanalysis. A simulation using default parameters produced adequate agreement with ERA5 reanalysis data (Figure 1).

Here we briefly look at the evolution of the event. Precipitating clouds associated with the low pressure system swept eastward through the region. Behind them, lightly-precipitating stratus clouds descended from an initial height of over 1000 m to a few hundred meters and, in some places, all the way to the ground. Figure 2 shows this process. The presence of clouds prior to fog

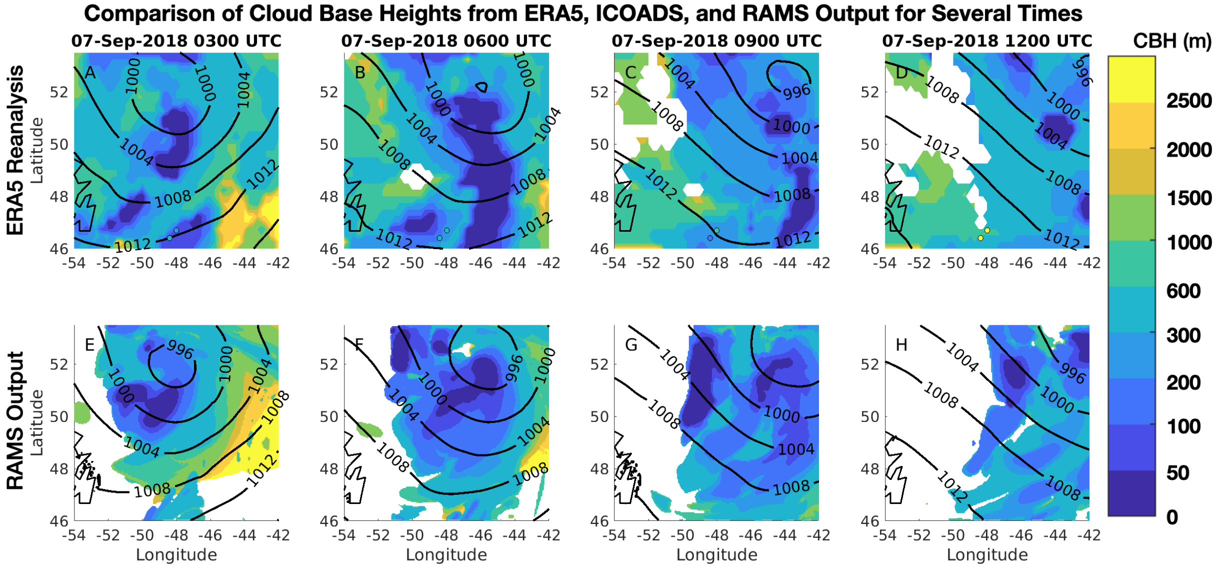

FIG. 1. Cloud base height and sea level pressure (black contours) at 4 hr intervals for the fog case ~~in~~ (A-D) in ERA5 reanalysis with ICOADS observations shown (colored circles) and (E-H) as simulated by RAMS.

onset indicates that fog can be classified either as precipitation fog or as cloud base lowering. The distinction between the two is subtle. In precipitation fog, there is typically an inversion-capped boundary layer that is cooled/moistened by precipitation falling through it from clouds above the inversion (Tardif 2007). In stratus-lowering fog, the cloud base is initially under the boundary layer capping inversion (Pilié et al. 1979). An observer at 49° N and 45° W would have seen cloud base descend at approximately 300 m per hour between 0300 and 0600 UTC. Cloud base at 45° W then remains low for 6 hours before the system eventually passes. In panel E of Figure 2 for 0900 UTC, we see low clouds forming under a dense, precipitating cloud towards the east, indicating precipitation fog, and also low clouds without precipitation forming above them. This shows that both precipitation fog and cloud-base lowering fog are present within our simulation.

b. Parameters

We chose to test the sensitivity of fog to aerosols, cloud droplet shape parameter, surface deposition rate parameterization, and sea surface roughness. Table 1 shows the variables tested and their ranges within the suite of simulations. The subsections below detail the motivation for choosing these parameters, the assumptions behind them, and why the parameter range was chosen.

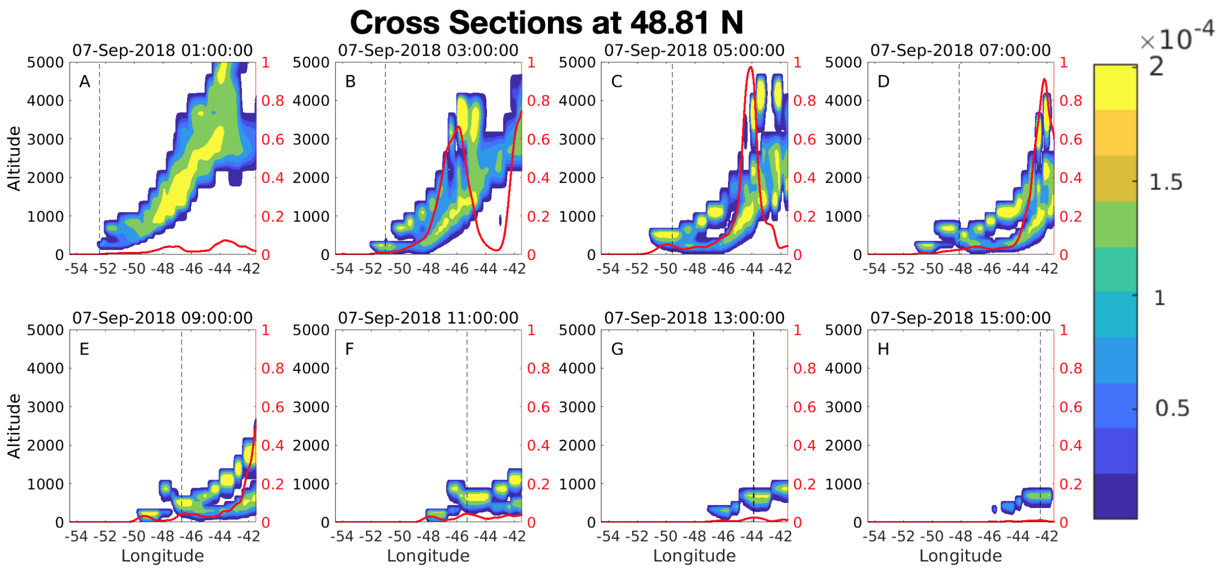

FIG. 2. Time series showing cross sections at 48.81 N of simulated cloud liquid water content (kg kg^{-1}) at 2 hour intervals. The vertical dashed line represents the transition between precipitation and stratus lowering fog regimes. The solid black line shows longitudinal mean precipitation rate within the domain with scale shown in mm/hr by orange numbers at the right of each subplot.

Parameter	Min	Max	Sampling (log or linear)
Aerosol Number Concentration	50 cm^{-3}	1000 cm^{-3}	Log
Mean Aerosol Diameter	10 nm	500 nm	Log
Shape Parameter (Microphysics)	2	10	Linear
Shape Parameter (Radiation)	2	10	Linear
Turbulent Deposition Enhancement	1	4	Linear
Surface Roughness α	0.01	0.1	Log

TABLE 1. Table of input parameters for sensitivity testing showing minimum value, maximum value, and logarithmic or linear sampling.

1) AEROSOLS

For coastal fog and land fog, particle concentrations play a major role in both the formation and properties of fog. Witiw and LaDochy (2008) hypothesized that the decrease in coastal fog events in California observed since the 1970s has been due in part to reduced air pollution, with another major factor being changes in SST (Witiw and LaDochy 2008; O'Brien et al. 2013). Studies have found a correlation between aerosol number concentration and fog for radiation fog (Maalick et al. 2016; Schwenkel and Maronga 2019) and marine fog formed where the air temperature is higher than SST (Wainwright and Richter 2021). Maalick et al. (2016) and Wainwright and Richter (2021) both find higher fog lifetime and liquid water content with higher aerosol concentration due to increased droplet activation (Gultepe and Isaac 1999).

We chose to vary both aerosol number concentration and mean aerosol diameter. Both of these serve to modify total aerosol mass concentration. In this study, we vary aerosol number concentration from 50-1000 cm^{-3}, which covers the range from typical (clean) marine aerosol concentrations to a reasonably polluted atmosphere. We expect most realistic situations for marine air masses to be towards the lower end of this range (Fitzgerald 1991). As for aerosol diameter, we used values between 10 and 500 nm. 10 nm is quite small and would correspond to the Aitken mode. We expect most realistic situations to be somewhere in the middle of this range. Both parameters are sampled logarithmically to attain greater sampling density at the lower ends of their ranges.

2) Shape Parameters

RAMS uses a double-moment bulk microphysics scheme which assumes a gamma size distribution for all hydrometeor species. Because this is a three-parameter distribution and we only predict two moments of the distribution, one parameter of the size distribution must be specified. As in many bulk schemes, the "shape parameter" is specified. The shape parameter is directly related to the relative width of a distribution; a lower shape parameter means a wider size distribution for a given mass and number concentration. In this study, we vary the shape parameter of the cloud droplet size distribution. The shape parameter of a droplet distribution impacts cloud properties and microphysical process rates, and thus cloud development (Igel and van den Heever 2017; Barthlott et al. 2022). In terms of microphysical processes, we expect that the droplet shape parameter will be important due to its effects on mean fall speed of droplet mass and number concentration and on collision-coalescence. Sensitivity to the cloud droplet shape parameter has been found in radiation fog previously (Boutle et al. 2022). The droplet shape parameter will also impact fog formation by changing the rate of cloud-top radiative cooling, which is thought to be important for stratus lowering fog (Pilié et al. 1979; Koračin et al. 2001). In order to capture the effects of microphysics and radiation separately, we used different assumed shape parameters for the microphysics and radiation parameterizations within the model. We varied the shape parameters used for both radiation ~~and~~ (referred to as microphysics and radiation shape parameters, respectively) and microphysics from 2 to 10, which is a realistic range for cloud droplet size distributions (Miles et al. 2000).

3) Deposition

When modeling clouds, it is typically assumed that the settling velocities of cloud droplets are negligible–except with respect to collisions for autoconversion. However, since fog occurs at the surface, gravitational settling leads to moisture loss through deposition. Findlater et al. (1989) found that loss of moisture to the surface is among the most important factors in the formation of marine fog off the coast of Scotland. Moisture loss to the surface through direct deposition of cloud droplets as well as drizzle can alter the properties of the fog (Mazoyer et al. 2017; Taylor 2021; Taylor et al. 2021). More generally, the fall speed of larger droplets causes them to fall out of fog, changing the fog's properties (Koračin et al. 2014).

In addition to the impact of gravitational settling, we expect fog droplet deposition to be enhanced through turbulence (Taylor 2021). In the absence of a body of work detailing exactly how turbulence might enhance settling and deposition, we decided to parameterize this process as a multiplicative enhancement on the gravitational settling velocity that only applies to the lowest model level (the lowest 10 m of the atmosphere). We used a range of 1 to 4 for our new turbulent deposition enhancement parameter. This range is reasonable given a typical cloud droplet settling velocity of 1 cm/s and the deposition velocity of about 4 cm/s calculated using Eq. 8 of Taylor (2021) using the height of our lowest scalar grid level (5 m) and 0.4 m/s for the friction velocity (this value is approximately the 90th percentile value in our simulations). Additionally, waves may increase surface deposition rates relative to gravitational settling velocity (Zufall et al. 1999), which has not been accounted for in the equation from Taylor (2021).

4) Sea Surface Roughness

Since marine fog has been shown to be sensitive to turbulence and mean wind at the surface (Fu et al. 2010), we investigated its sensitivity to marine surface roughness in addition to the microphysical parameter described above. Surface roughness impacts both mean wind and turbulence by creating drag, which leads to shearing and the mechanical generation of turbulence. RAMS uses the Charnock-Ellison relation (Charnock 1955). The Charnock-Ellison relation posits that marine surface roughness is a function of friction velocity, u_*. Specifically, $z_0 = \frac{\alpha}{g} u_*^2$, where α is a constant determined for each body of water . In RAMS, α is assumed to be 0.016 globally. However, more recent studies have offered other parameterizations of z_0 for the ocean that sometimes lead to dramatically higher roughness lengths, particularly in high-wind environments. For example (Taylor and Yelland 2001) presents a formula based on wave height and period.

Rather than implement a new parameterization for sea surface roughness, we decided to vary α within the Charnock-Ellison relation to reflect the overall uncertainty. We varied α from 0.01 to 0.1. Note that the default α, and indeed most calculated values of α, are towards the bottom of this range. As a result, we assume that realistic values of α will be towards the lower end of our range, but effective values near the upper end are possible under different environmental conditions.

c. Simulation Suite

The general methodology of this study follows that of Lee et al. (2011), Lee et al. (2013), Johnson et al. (2015) and others. We set up a suite of 78 simulations with different combinations of our input parameters. To do this, we used Latin Hypercube Sampling, which uses our different parameters as orthogonal bases for a 6-dimensional space and constructs a hypercube within that space bounded by the rages of our parameters. This allows us to sample our parameter space.

We also had the choice of whether to sample each parameter in log space or linear space. Sampling log space biases our samples towards the lower end of our range for a given parameter and is preferable when the sensitivity of the outputs to a parameter is expected to be greater at the lower end of the range. As discussed previously, aerosol number concentration, aerosol diameter, and surface roughness α are sampled logarithmically whereas the other input parameters are sampled linearly.

d. Output Variables

The fog present in our simulations needs to be described using a set of continuous values chosen to be as descriptive as possible. However, we first need to define fog. For our purposes, fog is when the presence of liquid water suspended in the air as cloud droplets reduces visibility ~~at 10 m above the surface (the first model level)~~ to less than 1 km ~~(WMO 1974)~~(WMO 1974; Koračin 2017) in the lowest model grid level. Following Stoelinga and Warner (1999), visibility is calculated as

3.912/β where β is the extinction in the visible band (245 - 700 nm) of the Harrington radiation parameterization (Harrington 1997). To quantify simulation fogginess, we used both superlatives and time-averaged quantities. Specifically, we examine the following six quantities:

1. The maximum spatial extent of the fog, found by counting the total number of grid cells defined to be foggy and then finding the maximum at any one time.

2. The difference between fog onset and dissipation times to quantify the duration of our fog event. Onset is defined when the fog condition is met anywhere in the domain except the 100 km nearest to the simulation edges due to nudging at the boundaries. Fog dissipation is defined using mean 10 m liquid water concentration. Specifically, we assume that the fog event is over when mean 10 m liquid water concentration drops below 5% of its maximum value. This is not strictly the end of the fog event. However, we found that small patches of fog may linger for hours after the majority of fog has dissipated and we did not feel that accounting for these patches best characterized the bulk behavior of the fog. ~~Therefore, we chose this alternative definition of fog dissipation~~Additionally, there were some cases where fog became mist and then more fog formed. To make onset and dissipation times consistent with the first onset and final dissipation of the main fog patches, we chose different onset and dissipation conditions. Onset and dissipation times are reported in ~~600 second~~ 10 minute intervals.

3. The time-integrated fog water, which effectively finds the mean fog spatial coverage and thickness derived from vertically-continuous cloudy cells up to 800 m, the approximate height of the capping inversion in our simulations.

4. The minimum visibility at the 10 m level achieved during the simulation.

5. The maximum 10 m droplet number concentration.

6. The maximum 10 m cloud water concentration.

The maximum fog extent and the fog duration together help to understand the fog water hours. Likewise, the maximum surface water concentration and droplet concentration can together help to explain the minimum visibility. Note that simulation output is available every 10 minutes to assess these quantities.

e. Gaussian Process Regression

Using these outputs, we create statistical emulators using the first 60 simulations in the simulation suite. To create each statistical emulator, we used Gaussian Process Regression to simultaneously fit all of our input parameters to each of our output values. Gaussian process regression, or kriging, is a non-parametric fitting approach that uses a stochastic process to interpolate a curve based on sampled points (Williams and Rasmussen 2006; Lee et al. 2011, 2013; Johnson et al. 2015). Kriging uses hyperparameters, like a covariance function, to tune the Bayesian interpolation process. We created models using the MATLAB Gaussian Process Regression tools with a large number of different basis function, kernel, and hyperparameter combinations and then evaluated these against each other to determine the best performer for use in our analysis. Model performance was evaluated based on several criteria and with the 18 reserved validator simulations. Specifically, the evaluation metrics included 1) the mean of the 95% confidence interval of the emulator's prediction for each data point normalized by the total data spread, 2) the fraction of validator points that fell within the 95% confidence intervals, 3) the fractional reduction of root mean squared error (RMSE) for the validator dataset relative to a constant function of the dataset mean, and 4) the correlation coefficient between emulator predictions the outputs of the validator simulations. These four scores, normalized confidence interval, confidence interval skill, RMSE reduction, and correlation coefficient, were constructed to range from 0 to 1 and then summed together to create a total score. For each output variable, the combination of fit parameters that produced the emulator with the highest total score was chosen for use in analysis.

3. Results

a. Overview

Figure 3 shows the performance of our best emulators in predicting the output values from our simulation suite in RAMS. There are no obvious systematic biases in the statistical emulators. The prediction-value pairs are distributed more-or-less evenly about the one-to-one line in all six subplots. It is worth noting that using machine learning to optimize fitting hyperparameters sometimes led to fitting the emulator dataset extremely accurately, causing all the points in blue to lie almost exactly on the one-to-one line. This likely indicates that we are overfitting the training data, and evidence of overfitting is apparent in some of the figures that follow. However, when evaluating the performance of our statistical emulator models, we looked primarily at how well it predicted the validator dataset, shown in red. Even in the cases of overfitting, the emulators predict the validator dataset reasonably well and we have confidence that they can correctly identify the primary factors that cause variance in the simulated fog properties.

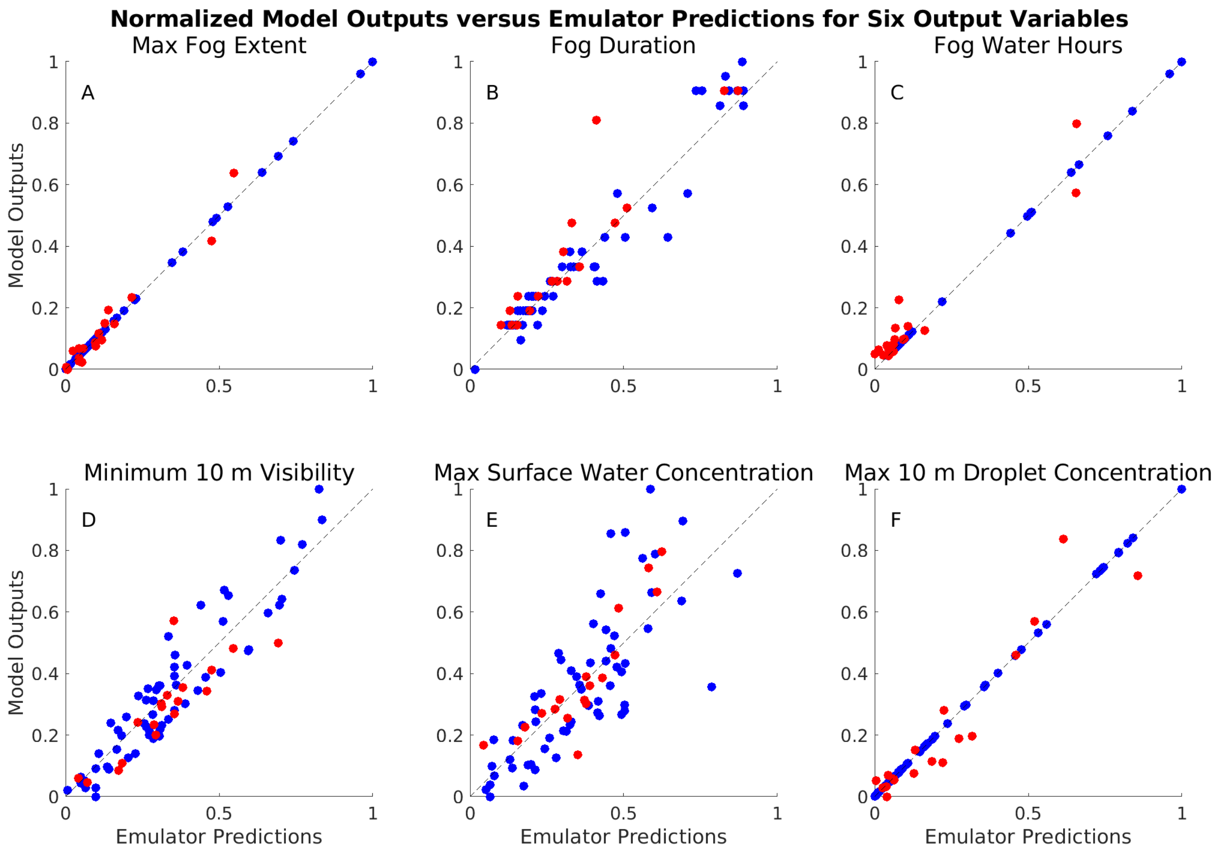

FIG. 3. Plots of emulator predictions versus RAMS output values for six output variables. Training datasets plotted in blue and validator sets plotted in red. Dashed one-to-one line displayed for reference.

Figure 4 shows partial dependence plots for all six fog properties on all of the input parameters. Partial dependence plots are created by fixing one input value and finding the average output value over every combination of the other five input values, then repeating this process over the full range of each input value until curves have been created for all of them. The difference between the maximum and minimum of each partial dependence curve gives the approximate total sensitivity of the output value to that input parameter. Mean aerosol diameter (blue) is typically the most important input parameter, which we can identify by the fact that it has the greatest difference between its minimum and maximum values in each partial dependence plot. Most of the sensitivity to the mean diameter is often for normalized values less than 0.2 which corresponds to mean diameters of 10 - 108 nm. These sizes are smaller than those typical for marine boundary layers (Porter and Clarke 1997) and as such the potential importance of the aerosol size is likely exaggerated in these results. Above about 100 nm, where aerosol sizes are more realistic, there is very little sensitivity to the aerosol size for most fog properties, and therefore, we won't focus too much on understanding the impacts of aerosol size. Microphysics shape parameter (red) is the next most important, followed by aerosol number concentration (black). We will focus on these two input parameters in the remainder of the discussion. The effects of radiation shape parameter (green), turbulent deposition enhancement (pink), and sea surface roughness α are generally small. While the latter three parameters appear less important than the former three, that does not mean that they do not impact fog. If only these parameters were varied, we would be able to see their impacts more clearly, but our simulations appear to show that aerosol number concentration and microphysical shape parameter have a far greater impact.

b. Minimum Visibility

The relationship between the input parameters and the minimum 10 m visibility align with expectations (Figure 4d). The turbulent deposition enhancement, which increases the gravitational settling rate for the lowest 10 m of the simulation, is positively correlated with minimum visibility. Put another way, a higher gravitational settling rate near the surface leads to more moisture flux out of this layer through deposition to the surface, leading to lower cloud liquid water concentration (magenta line in Figure 4e) and higher visibility (Figure 4d). The impact of the turbulent deposition enhancement comes primarily from the mass concentration of cloud liquid water concentration rather than the number concentration of cloud droplets (Figure 4f) due to its preferentially impacting larger droplets.

Higher aerosol number concentration and mean aerosol diameter are both positively correlated to 10 m cloud droplet concentration (black and blue lines, respectively, in Figure 4f) and max surface water concentration (Figure 4e). As a result, higher aerosol concentration and higher mean diameter are correlated to lower minimum visibility (Figure 4d). More aerosols and larger aerosol particles, which are easier to activate, lead to higher cloud droplet number concentration and lower

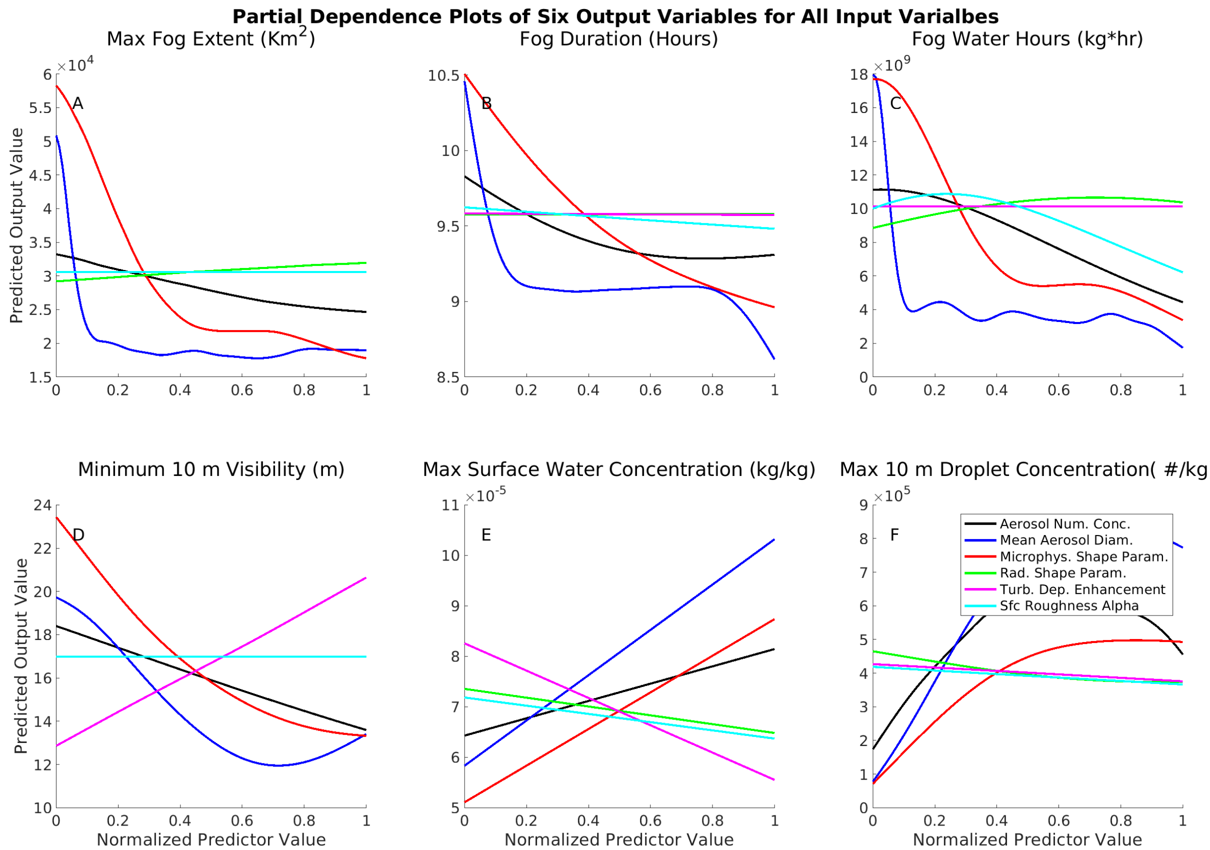

FIG. 4. Partial dependence plots for each of output variables with respect to all six input variables. All predictor values are normalized with their minima at zero and maxima at one on a linear scale. Note that the turbulent deposition enhancement line is obstructed by the surface roughness alpha line in panel A.

mean cloud droplet radius, which leads to less gravitational settling flux and more moisture content in the lowest 10 m.

The microphysics shape parameter is negatively correlated with minimum visibility (red line in Figure 4d). For a given number and mass concentration of droplets, a higher shape parameter means a narrower cloud droplet size distribution which in turn corresponds to two changes: a slower mass-weighted mean fall speed and reduced collision-coalescence. Both changes reduce the moisture loss to the surface, increasing the amount of cloud liquid water in the lowest 10 m.

In summary, minimum visibility is reduced by changes to the input parameters that lead to less gravitational settling and moisture loss to the surface, either directly through changes to turbulent deposition enhancement and microphysics shape parameter or indirectly through activation of more, smaller cloud droplets.

c. *Fog Extent*

The reasons for the sensitivity of fog extent, duration, and water hours to the input parameters are less apparent. The parameters that we have tested have the potential to impact the processes leading to formation and maintenance of fog as well as those leading to removal and dissipation of fog and all are important for controlling the fog extent and duration. As discussed previously, fog seems to have formed due both to precipitation and stratus cloud base lowering. The trends in fog with the input parameters may reflect local changes to these processes, but may also reflect changes to synoptic scale precipitation. Dissipation may be driven by a local cloud base rise, evaporation, and/or direction deposition to the surface. We will focus first on the direct deposition and the synoptic precipitation, and then discuss more local formation and dissipation processes.

Deposition of moisture on the surface represents a significant portion of the moisture budget of fog (Mazoyer et al. 2017). If changes to moisture loss through deposition were controlling the partial dependencies of fog properties (Figure 4), then higher aerosol number (which leads to smaller, more slowly falling droplets), higher microphysics shape parameter (which reduces drizzle production), and lower turbulent deposition enhancement all would presumably have led to reduced deposition to the surface and hence more fog. As already discussed, these reductions in deposition are certainly reflected when examining visibility and surface water concentration. However, the spatial extent of the fog is reduced, not increased, for both higher aerosol concentration and higher microphysics shape parameter. The turbulent deposition enhancement, meanwhile, was found to be unimportant. These results together suggest that fog water loss to the surface is not an important limiting factor for the fog extent or duration, perhaps due to low-level convergence providing a source of water vapor in the boundary layer (Boutle et al. 2010).

In terms of ~~synoptic~~ domain mean precipitation, a reasonable hypothesis is that fewer aerosols and a lower microphysics shape parameter (wider droplet distribution) enhance precipitation by increasing average droplet size and collision coalescence, moistening the boundary layer and promoting fog formation. Such a process could occur in the synoptic precipitation ahead of the fog formation, leading to a pre-moistening of the boundary layer, or it could happen locally in the low cloud deck trailing the synoptic precipitation.

Enhanced fog formation driven by greater synoptic precipitation is not borne out by the data. Figure 5 shows that the simulations with the most extensive fog also have above average synoptic precipitation, but that the highest-precipitation simulations did not produce the most fog. Instead, we see two regimes, a low fog extent regime with a weak correlation to precipitation, and a high fog extent regime that correlates negatively with precipitation. The high fog regime requires both low ~~aerosol size~~ mean aerosol diameter and low microphysics shape parameter. The negative correlation between fog extent and domain mean precipitation in the high fog regime is not related to fog losing moisture to the surface through the formation of drizzle and direct deposition of cloud droplets. Most of the precipitation precedes fog onset. Higher synoptic precipitation is not driving higher fog extent.

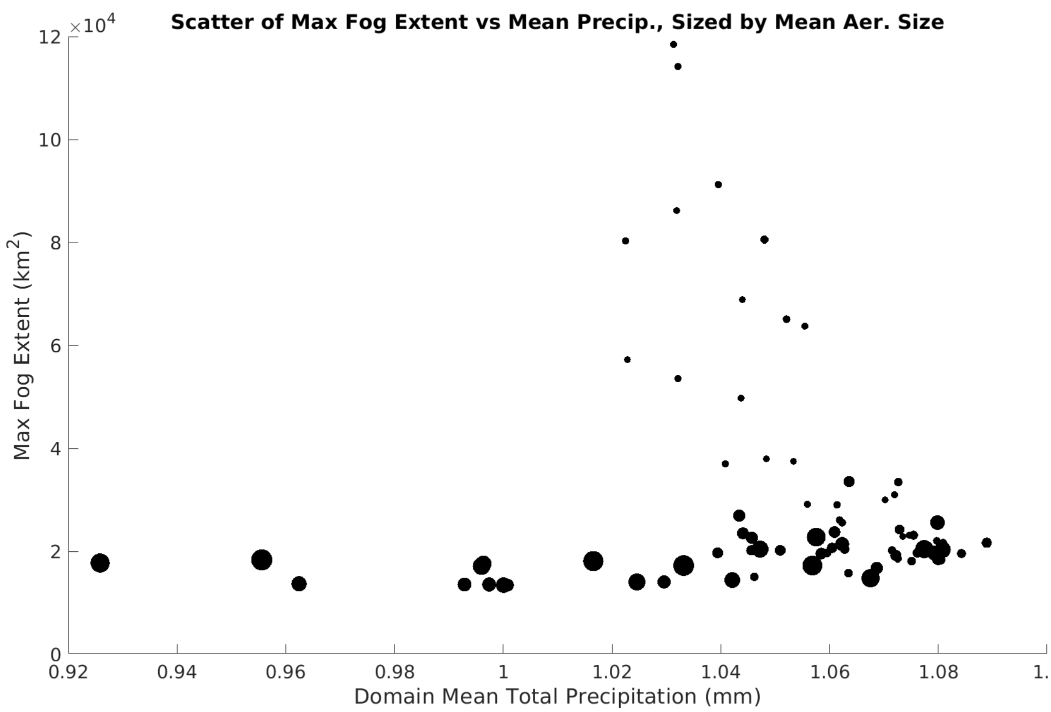

FIG. 5. Scatter plot of maximum fog extent versus domain mean accumulated precipitation, sized by mean aerosol size.

Perhaps then the relationship between microphysics and fog formation in this fog case is primarily driven by local precipitation effects. Figure 6 shows temperature, dew point, and precipitation over time for three points in each of three simulations, the most foggy, the closest-to-average foggy, and the least foggy. The plots suggest that light, local precipitation just ahead of fog formation is an important driver of fog formation in the early part of the simulation, but is not as significant in the second part of the simulation. This indicates that there are two fog formations, one that is precipitation-driven, and one that is not, as also discussed in Section 5.2.1.

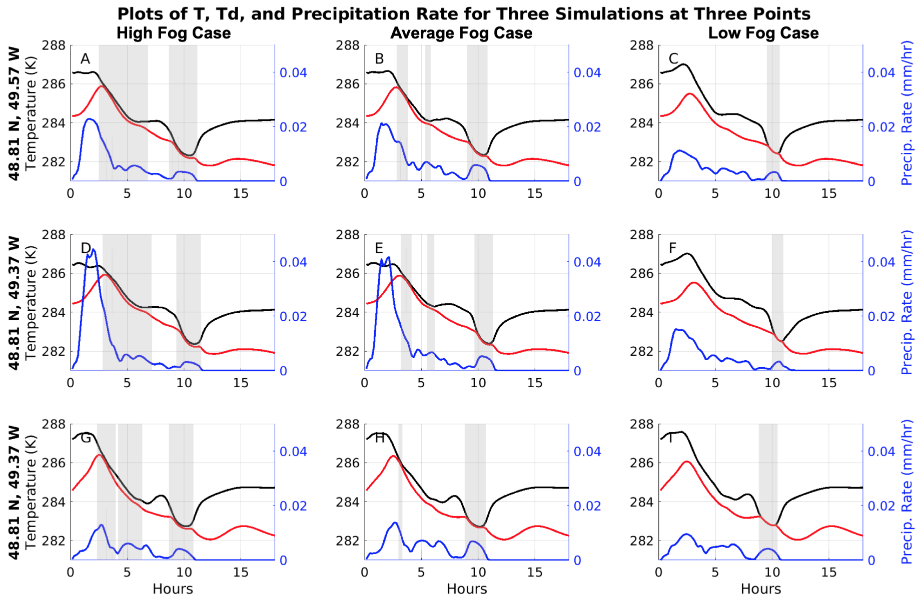

FIG. 6. Plot showing temperature (black) dew point temperature (dashed red), and precipitation rate (blue) for the foggiest simulation, the simulation closest to the mean fog water hours, and the least foggy simulation at locations corresponding to the foggiest points for each simulation. Shaded regions correspond to times when fog was present.

The two fog sub-events have different formation mechanisms. The first event appears to be precipitation fog while the second appears to be stratus lowering. Figure 7 shows temperature and dew point profiles for two sets of time series. The first time series compares ~~tests 60 and 67~~ the most and least foggy simulations for the first fog formation. A precipitating cloud moistens air below an inversion. In ~~test 60~~the high fog test, the air saturates all the way down to the surface, but this does not occur in ~~test 67.~~ the low fog test. This fog event forms in the manner of precipitation fog described by Tardif (2007). All simulations were broadly similar for the second time series (not shown), where a low cloud capped by an inversion grows downward until it contacts the surface, matching well with descriptions of stratus lowering fog (Oliver et al. 1978; Pilié et al. 1979). Since we appear to have fog forming by different mechanisms, we next attempt to separately assess the importance of the input parameters on each fog type and further explore the role of local processes in explaining the dependencies on these parameters.

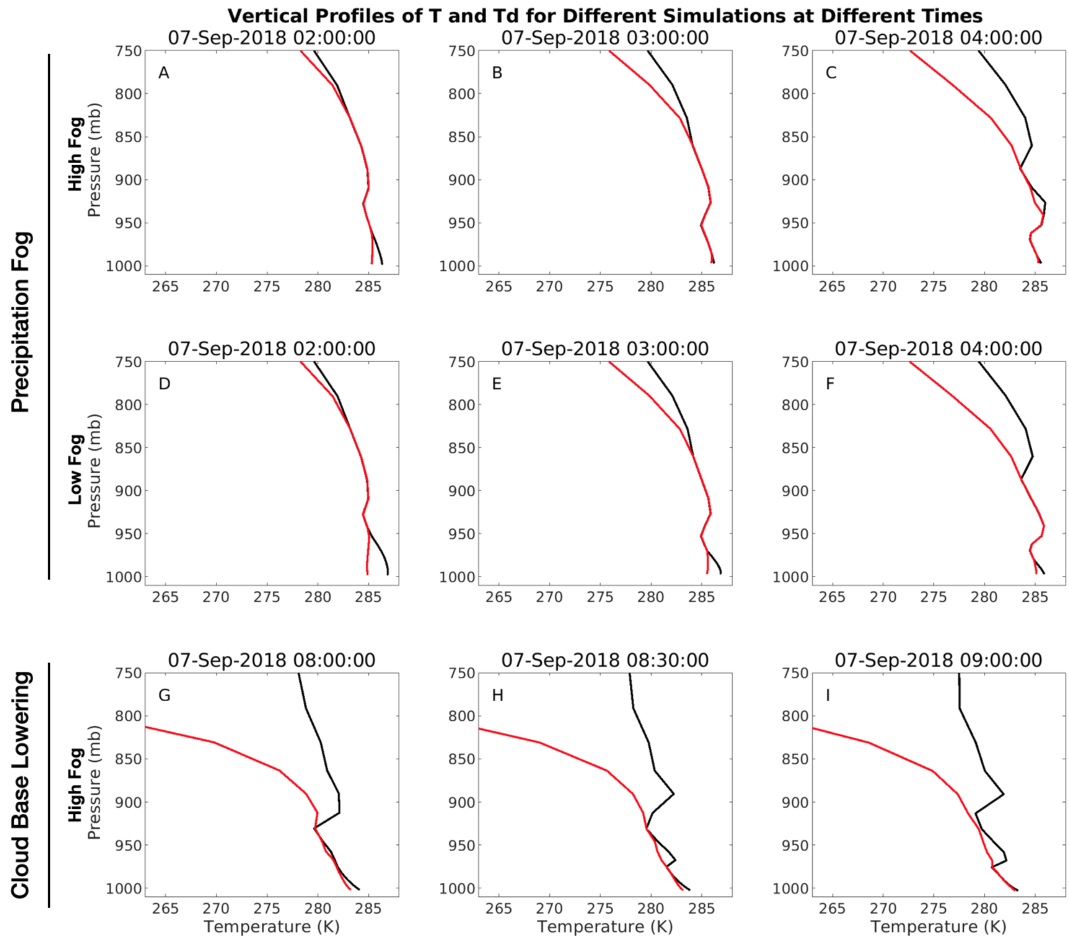

FIG. 7. Vertical profiles of temperature and dew point showing fog formation or lack thereof during two time series. The first fog formation, hypothesized to be precipitation fog, occurred in ~~high fog~~ most foggy test ~~(60)~~ but not in ~~low fog~~ least foggy test~~(67)~~. The second fog formation is hypothesized to be cloud base lowering and occurred in all simulations.

Sub-Event Microphysical Dependencies

To investigate the two fog sub-events individually, we separate the simulation domain using a dividing line that moves eastward at a specified rate of 33 km/hr such that it falls between the two fog banks. We then performed the same sensitivity testing procedure on both the precipitation fog and the cloud base lowering fog separately. The resulting partial dependence plots are shown in figure 8. The emulator struggled with overfitting the cloud base lowering fog with respect to aerosol diameter, but inspection of the validation tests indicates that the emulator is nonetheless performing well (not shown).

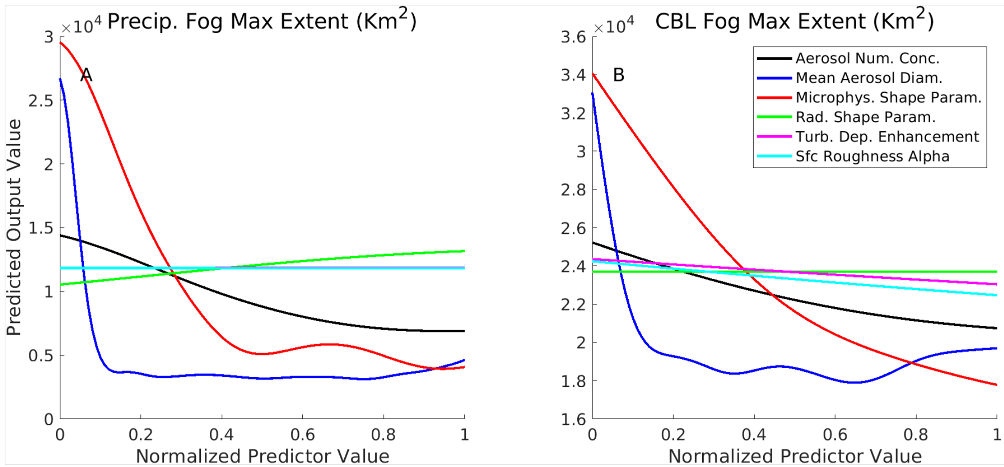

FIG. 8. Partial dependence plots of maximum fog extent and minimum visibility for the precipitation fog and cloud base lowering (CBL) fog formation sub-events.

Figure 6 anecdotally suggests that cases with more fog overall tend to have more fog in both sub-events and that each fog type depends on the input parameters in broadly similar ways. Indeed, the maximum fog extents of each sub event are strongly correlated to each other (not shown). However, the early, precipitation fog sub-event is far more sensitive to our input parameters (Figure 8). Specifically, if we look at the ranges of our output parameters for each sub-event, we see roughly twice the range for precipitation maximum fog extent than cloud base lowering maximum fog extent. This shows that precipitation fog is the main source of spread between the models in terms of fog amount (Figure 4).

We find that precipitation fog is strongly related to mean below-cloud evaporation prior to fog onset, calculated as the mean evaporation east of the dividing line at the 10 m level, where precipitation fog extent is greater for more evaporation (Figure 9a). Notably, the simulations with the highest evaporation did not have the highest precipitation, both domain-wide and just ahead of fog onset. Rather, consistent with the sensitivity of fog extent (Figure 8a), more evaporation is associated with a smaller microphysics shape parameter and lower aerosol concentrations (Figure 9b). Both of these conditions should favor the production of drizzle within the cloud which subsequently evaporates below cloud base. Because evaporation is strong, the drizzle doesn't necessarily reach the surface and these simulations don't necessarily have the largest local precipitation accumulations. Finally, if the mean below-cloud evaporation is included as a predictor in the emulator, then we see that it accounts for most of the differences among simulations, with only microphysics shape parameter having an appreciable independent impact. This independent impact could possibly come from the direct influence of the microphysics shape parameter on evaporation rates. Igel and van den Heever (2017) found that cloud water with an underlying droplet ~~distributions~~ distribution characterized by a high shape ~~parameters~~ parameter will evaporate more quickly and that this increased evaporation rate is associated with reduced cloud fraction in shallow cumulus clouds. It is possible that a similar process is occurring here to limit fog extent when the shape parameter is high (Figure 8a and 9).

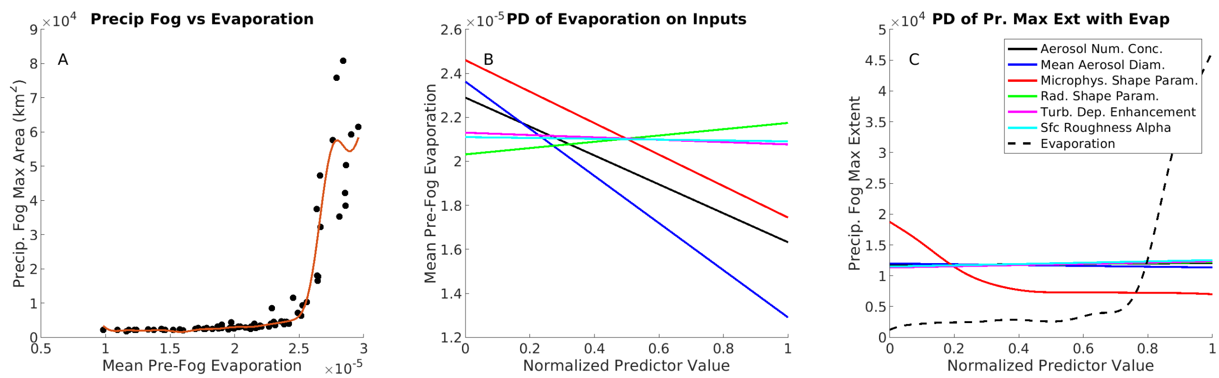

FIG. 9. Plots showing the relationship of mean 10 m evaporation east of the dividing line to max fog extent alone (left), the dependence of evaporation on all six input parameters (center), and a partial dependence plot of max fog extent on all input parameters with evaporation included as an extra predictor (right)

The cloud base lowering fog extent is dependent on the input parameters in a way that is very similar to precipitation fog (Figure 8). This may be because cloud base lowering fog is also influenced by sub-cloud evaporation processes or possibly because the precipitation primes the environment for the subsequent cloud base lowering fog. To test the extent to which the second, cloud base lowering sub-event is dependent on the precipitation fog that precedes it, we take the mean 10 m relative humidity at the dividing line described earlier (line RH) as a proxy for the conditions left behind by the precipitation fog. This line RH is then used as an input to the emulator. This gives us a way to isolate the impacts of our input parameters on cloud base lowering fog, albeit an imperfect one due to the relationship between our inputs and line RH.

Gaussian process regression of our input parameters and line RH yields the partial dependence plots shown in figure 10. Line RH is the most important factor in determining the amount of fog

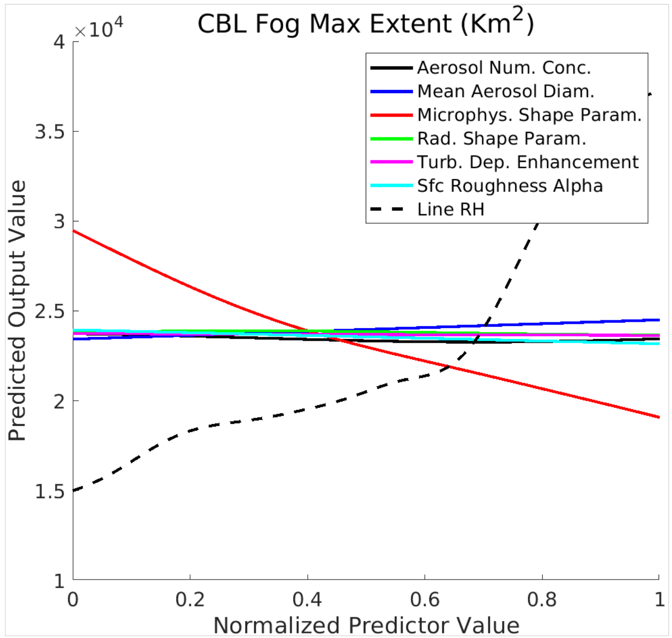

481 FIG. 10. Partial dependence of cloud base lowering fog on all input parameters as well as the average relative humidity at the dividing line between the precipitation and cloud base lowering sub-events.

formed through cloud base lowering. More fog formation early in the simulation leads to higher relative humidity near the surface, which in turn enhances fog formation later in the simulation. Of the other parameters, only microphysics shape parameter remains significant. Microphysics shape parameter maintains its negative correlation to fogginess, much as it did for precipitation fog after sub-cloud evaporation is accounted for (Figure 9c). The reasons are unclear, but they could be related to changes in fog evaporation or possibly processes within the lowering cloud. Finally, despite the importance for cloud top radiative cooling in driving cloud base lowering (Koračin et al. 2005a), this fog does not strongly depend on the radiation shape parameter. This may be because the shape parameter simply does not modify cloud top cooling rates enough to have a large impact, or that perhaps processes other than radiative cooling were more important for driving the fog formation.

4. Conclusion

This study examined the sensitivity of a marine fog event that occurred on 7 September 2018 over the Grand Banks to six microphysical and turbulent parameters. Fog formation was driven by a passing front and occurred in two distinct sub-events with different formation mechanisms. The first sub-event formed as light precipitation from above evaporated in the boundary layer, moistening the layer until it became saturated all the way down to the surface, creating fog. The second fog formation resulted from low stratus clouds behind the front and capped by the top of the boundary layer growing downwards until they reached the surface. Both fog types are driven by the downward flux of liquid water. As a result, their sensitivities to microphysical input parameters correspond to parameter combinations that typically lead to fewer, larger droplets that tend to descend more quickly. Lower minimum 10 m visibility, which occurs when gravitational settling flux is lower and less moisture is lost to the surface, is related to a lower spatial and temporal extent of fog.

Among the input parameters, microphysics shape parameter is the most important. Mean aerosol size has the greatest overall effect between its minimum and maximum values, but the sensitivity of fog properties is confined to mean aerosol sizes between 10 and 50 nm, meaning that it is probably irrelevant in real-world contexts. This leaves aerosol number concentration and microphysics shape parameter as the two most important parameters, with the latter having a substantially larger effect overall. Previous studies have found radiation fog to be sensitive to aerosol (Maalick et al. 2016; Schwenkel and Maronga 2019; Wainwright and Richter 2021). These studies reported increased fog with higher aerosol content, which is consistent with the minimum visibility trends from this study. However, they also found increases in the fog lifetime, whereas here we see reduced fog lifetimes and fog extents. Likely the difference is linked to the different types of fog studied and it highlights the importance of studying different fog formation mechanisms independently.

The impact of the shape parameter of the cloud droplet size distribution is less well established, but this case study indicates that it strongly impacts the behavior of fog. A narrower cloud droplet size distribution is a distribution with a lower mean mass-weighted fall speed and one that will have less collision-coalescence, leading to reduced drizzle formation. As such, and as was also seen in radiation fog (Boutle et al. 2022), a narrower droplet size distribution decreases visibility at the surface. In our study it also decreases fog extent and lifetime. The impacts of the shape parameter on fog formation occur almost exclusively through microphysical processes rather than its direct impact on the radiative properties of the cloud/fog system. Additionally, microphysics shape parameter was the only input to have a significant independent impact on both the precipitation and stratus lowering fog independent of either the relative humidity of the boundary layer between the sub-events or by the boundary-layer evaporation prior to initial fog onset.

The substantial impact of microphysics shape parameter on fog in this set of simulations indicates that better understanding and treatment of the cloud droplet size distribution as it pertains to fog is an important area of further research. While measurements of the droplet size distribution in fog are common, it is difficult to find quantification of the distribution width in the literature and we are uncertain what the most realistic values of the shape parameter are. Additionally, the observed bimodal size distribution found in many fog cases (Pinnick et al. 1978; Niu et al. 2012) may play a significant role in the life-cycle of a fog case, requiring further research.

Acknowledgments. This work was supported by the Office of Naval Research grant N00014-20-1-2304-0.

Data availability statement. Model output every ten minutes for cloud water mixing ratio, cloud droplet number concentration, and visibility is available at `https://farm.cse.ucdavis.edu/~aigel/fog_mwr_2022`. Full model output is available every hour upon request, but due to the size of the dataset (>2 TB) is not openly available.

References

, 2018: International comprehensive ocean atmosphere data set (icoads) and ncei global marine observations.

Anderson, J. B., 1931: Observations from airplanes of cloud and fog conditions along the southern california coast. *Mon. Wea. Rev.*, **59 (7)**, 264–270.

Barthlott, C., A. Zarboo, T. Matsunobu, and C. Keil, 2022: Importance of aerosols and shape of the cloud droplet size distribution for convective clouds and precipitation. *Atmospheric Chemistry and Physics*, **22 (3)**, 2153–2172.

Boutle, I., R. Beare, S. E. Belcher, A. Brown, and R. S. Plant, 2010: The moist boundary layer under a mid-latitude weather system. *Boundary-layer meteorology*, **134**, 367–386.

Boutle, I., J. Price, I. Kudzotsa, H. Kokkola, and S. Romakkaniemi, 2018: Aerosol–fog interaction and the transition to well-mixed radiation fog. *Atmospheric Chemistry and Physics*, **18 (11)**, 7827–7840.

Boutle, I., and Coauthors, 2022: Demistify: a large-eddy simulation (les) and single-column model (scm) intercomparison of radiation fog. *Atmospheric Chemistry and Physics*, **22 (1)**, 319–333.

Charnock, H., 1955: Wind stress on a water surface. *Quart. J. Roy. Meteor. Soc.*, **81 (350)**, 639–640.

Dorman, C. E., A. A. Grachev, I. Gultepe, and H. J. Fernando, 2021a: Toward improving coastal-fog prediction (c-fog). Springer, 167–170 pp.

Dorman, C. E., S. W. Hoch, I. Gultepe, Q. Wang, R. T. Yamaguchi, H. Fernando, and R. Krishnamurthy, 2021b: Large-scale synoptic systems and fog during the c-fog field experiment. *Boundary-Layer Meteorology*, **181 (2)**, 171–202.

Duynkerke, P. G., 1999: Turbulence, radiation and fog in dutch stable boundary layers. *Boundary-Layer Meteorology*, **90 (3)**, 447–477.

Fernando, H. J., and Coauthors, 2021: C-fog: life of coastal fog. *Bulletin of the American Meteorological Society*, **102 (2)**, E244–E272.

Findlater, J., W. Roach, and B. McHugh, 1989: The haar of north-east scotland. *Quart. J. Roy. Meteor. Soc.*, **115 (487)**, 581–608.

Fitzgerald, J. W., 1991: Marine aerosols: A review. *Atmospheric Environment. Part A. General Topics*, **25 (3-4)**, 533–545.

Fu, G., P. Li, J. G. Crompton, J. Guo, S. Gao, and S. Zhang, 2010: An observational and modeling study of a sea fog event over the yellow sea on 1 august 2003. *Meteor. Atmos. Phys.*, **107 (3)**, 149–159.

Goldman, L., 1951: On forecasting ceiling lowering during continuous rain. *Mon. Wea. Rev.*, **79 (7)**, 133–142.

Gultepe, I., and G. Isaac, 1999: Scale effects on averaging of cloud droplet and aerosol number concentrations: Observations and models. *Journal of Climate*, **12 (5)**, 1268–1279.

Gultepe, I., G. Isaac, W. Leaitch, and C. Banic, 1996: Parameterizations of marine stratus microphysics based on in situ observations: Implications for gcms. *J. Climate*, **9 (2)**, 345–357.

Gultepe, I., and J. Milbrandt, 2007: Microphysical observations and mesoscale model simulation of a warm fog case during fram project. *Fog and boundary layer clouds: Fog visibility and forecasting*, Springer, 1161–1178.

Gultepe, I., and Coauthors, 2007: Fog research: A review of past achievements and future perspectives. *Pure Appl. Geophys.*, **164 (6-7)**, 1121–1159.

Gultepe, I., and Coauthors, 2009: The fog remote sensing and modeling field project. *Bull. Amer. Meteor. Soc.*, **90 (3)**, 341–360.

Haeffelin, M., and Coauthors, 2010: Parisfog: Shedding new light on fog physical processes. *Bull. Amer. Meteor. Soc.*, **91 (6)**, 767–783.

Harrington, J. Y., 1997: The effects of radiative and microphysical processes on simulation of warm and transition season Arctic stratus. PhD, Colorado State University, URL AvailablefromtheDepartmentofAtmosphericScience,ColoradoStateUniversity, FortCollins,CO80523, publication Title: Department of Atmospheric Science Volume: PhD.

Heo, K.-Y., and K.-J. Ha, 2010: A coupled model study on the formation and dissipation of sea fogs. *Mon. Wea. Rev.*, **138 (4)**, 1186–1205.

Hersbach, H., and Coauthors, 2020: The era5 global reanalysis. *Quart. J. Roy. Meteor. Soc.*, **146 (730)**, 1999–2049, https://doi.org/https://doi.org/10.1002/qj.3803, URL https://rmets.onlinelibrary.wiley.com/doi/abs/10.1002/qj.3803, https://rmets.onlinelibrary.wiley.com/doi/pdf/10.1002/qj.3803.

Huang, H., H. Liu, J. Huang, W. Mao, and X. Bi, 2015: Atmospheric boundary layer structure and turbulence during sea fog on the southern china coast. *Mon. Wea. Rev.*, **143 (5)**, 1907–1923.

Igel, A. L., and S. C. van den Heever, 2017: The importance of the shape of cloud droplet size distributions in shallow cumulus clouds. part ii: Bulk microphysics simulations. *J. Atmos. Sci.*, **74 (1)**, 259–273.

Johnson, J., Z. Cui, L. Lee, J. Gosling, A. Blyth, and K. Carslaw, 2015: Evaluating uncertainty in convective cloud microphysics using statistical emulation. *Journal of Advances in Modeling Earth Systems*, **7 (1)**, 162–187.

Kim, C. K., and S. S. Yum, 2012: A numerical study of sea-fog formation over cold sea surface using a one-dimensional turbulence model coupled with the weather research and forecasting model. *Boundary-Layer Meteorology*, **143 (3)**, 481–505.

Kim, C. K., and S. S. Yum, 2013: A study on the transition mechanism of a stratus cloud into a warm sea fog using a single column model pafog coupled with wrf. *Asia-Pacific Journal of Atmospheric Sciences*, **49 (2)**, 245–257.

Koračin, D., 2017: Modeling and forecasting marine fog. *Marine fog: challenges and advancements in observations, modeling, and forecasting*, Springer, 425–475.

Koračin, D., J. A. Businger, C. E. Dorman, and J. M. Lewis, 2005a: Formation, evolution, and dissipation of coastal sea fog. *Boundary-Layer Meteorology*, **117 (3)**, 447–478.

Koračin, D., C. E. Dorman, J. M. Lewis, J. G. Hudson, E. M. Wilcox, and A. Torregrosa, 2014: Marine fog: A review. *Atmos. Res.*, **143**, 142–175.

Koračin, D., D. F. Leipper, and J. M. Lewis, 2005b: Modeling sea fog on the us california coast during a hot spell event. *Geofizika*, **22 (1)**, 59–82.

Koračin, D., J. Lewis, W. T. Thompson, C. E. Dorman, and J. A. Businger, 2001: Transition of stratus into fog along the california coast: Observations and modeling. *J. Atmos. Sci.*, **58 (13)**, 1714–1731.

Lee, L., K. Carslaw, K. Pringle, G. Mann, and D. Spracklen, 2011: Emulation of a complex global aerosol model to quantify sensitivity to uncertain parameters. *Atmospheric Chemistry and Physics*, **11 (23)**, 12 253–12 273.

Lee, L., K. Pringle, C. Reddington, G. Mann, P. Stier, D. Spracklen, J. Pierce, and K. Carslaw, 2013: The magnitude and causes of uncertainty in global model simulations of cloud condensation nuclei. *Atmospheric Chemistry and Physics*, **13 (17)**, 8879–8914.

Leipper, D. F., 1994: Fog on the us west coast: A review. *Bull. Amer. Meteor. Soc.*, **75 (2)**, 229–240.

Lewis, J., D. Koračin, and K. Redmond, 2004: Sea fog research in the united kingdom and united states: A historical essay including outlook. *Bull. Amer. Meteor. Soc.*, **85 (3)**, 395–408.

Maalick, Z., T. Kühn, H. Korhonen, H. Kokkola, A. Laaksonen, and S. Romakkaniemi, 2016: Effect of aerosol concentration and absorbing aerosol on the radiation fog life cycle. *Atmospheric Environment*, **133**, 26–33.

Mazoyer, M., C. Lac, O. Thouron, T. Bergot, V. Masson, and L. Musson-Genon, 2017: Large eddy simulation of radiation fog: impact of dynamics on the fog life cycle. *Atmospheric Chemistry and Physics*, **17 (21)**, 13 017–13 035.

Miles, N. L., J. Verlinde, and E. E. Clothiaux, 2000: Cloud droplet size distributions in low-level stratiform clouds. *J. Atmos. Sci.*, **57 (2)**, 295–311.

Niu, S., D. Liu, L. Zhao, C. Lu, J. Lü, and J. Yang, 2012: Summary of a 4-year fog field study in northern nanjing, part 2: Fog microphysics. *Pure Appl. Geophys.*, **169 (5)**, 1137–1155.

Oliver, D., W. Lewellen, and G. Williamson, 1978: The interaction between turbulent and radiative transport in the development of fog and low-level stratus. *J. Atmos. Sci.*, **35 (2)**, 301–316.

O'Brien, T. A., L. C. Sloan, P. Y. Chuang, I. C. Faloona, and J. A. Johnstone, 2013: Multidecadal simulation of coastal fog with a regional climate model. *Climate Dyn.*, **40 (11-12)**, 2801–2812.

Pilié, R., E. Mack, C. Rogers, U. Katz, and W. Kocmond, 1979: The formation of marine fog and the development of fog-stratus systems along the california coast. *J. Appl. Meteor. Climatol.*, **18 (10)**, 1275–1286.

Pinnick, R. G., D. Hoihjelle, G. Fernandez, E. Stenmark, J. Lindberg, G. Hoidale, and S. Jennings, 1978: Vertical structure in atmospheric fog and haze and its effects on visible and infrared extinction. *J. Atmos. Sci.*, **35 (10)**, 2020–2032.

Porter, J. N., and A. D. Clarke, 1997: Aerosol size distribution models based on in situ measurements. *J. Geophys. Res.: Atmospheres*, **102 (D5)**, 6035–6045.

Reynolds, R. W., T. M. Smith, C. Liu, D. B. Chelton, K. S. Casey, and M. G. Schlax, 2007: Daily High-Resolution-Blended Analyses for Sea Surface Temperature. *J. Climate*, **20 (22)**, 5473 – 5496, https://doi.org/10.1175/2007JCLI1824.1, URL https://journals.ametsoc.org/view/journals/clim/20/22/2007jcli1824.1.xml, place: Boston MA, USA Publisher: Amer. Meteor. Soc.

Saleeby, S. M., and S. C. van den Heever, 2013: Developments in the CSU-RAMS Aerosol Model: Emissions, Nucleation, Regeneration, Deposition, and Radiation. *J. Appl. Meteor. Climatol.*, **52 (12)**, 2601–2622, https://doi.org/10.1175/jamc-d-12-0312.1.

Schwenkel, J., and B. Maronga, 2019: Large-eddy simulation of radiation fog with comprehensive two-moment bulk microphysics: impact of different aerosol activation and condensation parameterizations. *Atmospheric Chemistry and Physics*, **19 (10)**, 7165–7181.

Smagorinsky, J., 1963: General Circulation Experiments with the Primitive Equations. *Mon. Wea. Rev.*, **91 (3)**, 99–164, https://doi.org/10.1175/1520-0493(1963)091<0099:GCEWTP>2.3.CO;2, URL http://journals.ametsoc.org/doi/abs/10.1175/1520-0493(1963)091<0099:GCEWTP>2.3.CO;2.

Stoelinga, M. T., and T. T. Warner, 1999: Nonhydrostatic, Mesobeta-Scale Model Simulations of Cloud Ceiling and Visibility for an East Coast Winter Precipitation Event. *J. Appl. Meteor.*, **38 (4)**, 385 – 404, https://doi.org/10.1175/1520-0450(1999)038<0385:NMSMSO>2.0.CO;2, URL https://journals.ametsoc.org/view/journals/apme/38/4/1520-0450_1999_038_0385_nmsmso_2.0.co_2.xml, place: Boston MA, USA Publisher: Amer. Meteor. Soc.

Tardif, R., and R. M. Rasmussen, 2008: Process-oriented analysis of environmental conditions associated with precipitation fog events in the new york city region. *J. Appl. Meteor. Climatol.*, **47 (6)**, 1681–1703.

Tardif, R., and R. M. Rasmussen, 2010: Evaporation of nonequilibrium raindrops as a fog formation mechanism. *J. Atmos. Sci.*, **67 (2)**, 345–364.

Tardif, R. M., 2007: *Characterizing fog and the physical mechanisms leading to its formation during precipitation in a coastal area of the northeastern United States*. University of Colorado at Boulder.

Taylor, G., 1917: The formation of fog and mist. *Quart. J. Roy. Meteor. Soc.*, **43 (183)**, 241–268.

Taylor, P. A., 2021: Constant flux layers with gravitational settling: links to aerosols, fog and deposition velocities. *Atmospheric Chemistry and Physics*, **21 (24)**, 18 263–18 269.

Taylor, P. A., Z. Chen, L. Cheng, S. Afsharian, W. Weng, G. A. Isaac, T. W. Bullock, and Y. Chen, 2021: Surface deposition of marine fog and its treatment in the weather research and forecasting (wrf) model. *Atmospheric Chemistry and Physics*, **21 (19)**, 14 687–14 702.

Taylor, P. K., and M. J. Yelland, 2001: The dependence of sea surface roughness on the height and steepness of the waves. *J. Phys. Oceanogr.*, **31 (2)**, 572–590.

Wagh, S., R. Krishnamurthy, C. Wainwright, S. Wang, C. E. Dorman, H. J. Fernando, and I. Gultepe, 2021: Study of stratus-lowering marine-fog events observed during c-fog. *Boundary-Layer Meteorology*, **181 (2)**, 317–344.

Wainwright, C., and D. Richter, 2021: Investigating the sensitivity of marine fog to physical and microphysical processes using large-eddy simulation. *Boundary-Layer Meteorology*, **181 (2)**, 473–498.

Walko, R. L., and Coauthors, 2000: Coupled atmosphere, biophysics and hydrology models for environmental modeling. *J. Appl. Meteor.*, **39**, 931–944, https://doi.org/10.1175/1520-0450(2000)039<0931:CABHMF>2.0.CO;2.

Willett, H. C., 1928: Fog and haze, their causes, distribution, and forecasting. *Mon. Wea. Rev.*, **56 (11)**, 435–468.

Williams, C. K., and C. E. Rasmussen, 2006: *Gaussian processes for machine learning*, Vol. 2. MIT press Cambridge, MA.

Witiw, M., and S. LaDochy, 2008: Trends in fog frequencies in the los angeles basin. *Atmos. Res.*, **87 (3-4)**, 293–300.

WMO, 1974: Manual on codes, volume 1—international codes. WMO Publications Geneva.

Zhao, L., S. Niu, Y. Zhang, and F. Xu, 2013: Microphysical characteristics of sea fog over the east coast of leizhou peninsula, china. *Adv. in Atmospheric Sciences*, **30 (4)**, 1154–1172.

Zufall, M. J., W. Dai, and C. I. Davidson, 1999: Dry deposition of particles to wave surfaces: Ii. wind tunnel experiments. *Atmospheric Environment*, **33 (26)**, 4283–4290.